Article

Not peer-reviewed version

Bifunctional MoS2/Al2O3-zeolite catalysts in hydroprocessing of methyl palmitate

Evgeniya Vlasova * , Yiheng Zhao , Irina Danilova , Pavel Aleksandrov , Ivan Shamanaev , Alexey Nuzhdin , Evgeniy Suprun , Vera Pakharukova , Dmitry Tsaplin , Anton Maximov , Galina Bukhtiyarova

Posted Date: 19 September 2023

doi: 10.20944/preprints202309.1239.v1

Keywords: bio-jet fuel; MoS2 catalyst; zeolite; Brønsted acid sites; hydrodeoxygenation; hydroisomerization; methyl palmitate

Article

Bifunctional MoS_2/Al_2O_3-Zeolite Catalysts in Hydroprocessing of Methyl Palmitate

Evgeniya Vlasova [1,*], Yiheng Zhao [2], Irina Danilova [1], Pavel Aleksandrov [1], Ivan Shamanaev [1], Alexey Nuzhdin [1], Evgeniy Suprun [1], Vera Pakharukova [1], Dmitriy Tsaplin [3,4], Anton Maksimov [3,4], Galina Bukhtiyarova [1]

[1] Boreskov Institute of Catalysis SB RAS, 630090 Novosibirsk, Russia
[2] Novosibirsk National Research University, 630090 Novosibirsk, Russia
[3] Lomonosov Moscow State University, 119991 Moscow, Russia
[4] Topchiev Institute of Petrochemical Synthesis RAS, 119991 Moscow, Russia
* Correspondence: evgenia@catalysis.ru

Abstract: Series of bifunctional catalysts, MoS_2/Al_2O_3(70 wt.%)-zeolite (30 wt.%) (zeolite – ZSM-5, ZSM-12, ZSM-22 and silica aluminophosphate SAPO-11), were synthesized for hydroconversion of methyl palmitate (10 wt.% in dodecane) in a trickle-bed reactor. Mo loading was about 7 wt.%. Catalyst and supports were characterized by different physical-chemical methods (HRTEM-EDX, SEM-EDX, XRD, N_2 physisorption, FTIR spectroscopy). Hydroprocessing was performed at temperature of 250-350°C, hydrogen pressure 3.0-5.0 MPa, liquid hourly space velocity (LHSV) 36 h^{-1}, H_2/feed ratio – 600 Nm^3/m^3. Complete conversion of oxygen-containing compounds was achieved at temperature 310°C in the presence of MoS_2/Al_2O_3-zeolite catalysts, the selectivity for the conversion of methyl palmitate via the 'direct' hydrodeoxygenation (HDO) route was over 85%. The yield of iso-alkanes gradually increases in order: MoS_2/Al_2O_3 < MoS_2/Al_2O_3-ZSM-12 < MoS_2/Al_2O_3-ZSM-5 < MoS_2/Al_2O_3-SAPO-11 < MoS_2/Al_2O_3-ZSM-22. The sample MoS_2/Al_2O3-ZSM-22 demonstrated the highest yield of iso-alkanes (40%). Hydroisomerization activity of the catalysts was in a good correlation with concentration of Brønsted acid sites of synthesized supports.

Keywords: bio-jet fuel, MoS_2 catalyst, zeolite, Brønsted acid sites, hydrodeoxygenation, hydroisomerization, methyl palmitate

1. Introduction

Negative climate change caused by greenhouse gas emissions stimulate widespread expansion of the concept of "decarbonization" of the economy by reducing CO_2 emissions. One of the approaches to solve this problem in the transport sector is the use of renewable bio resources to obtain biofuel components that are not inferior in quality to products of petroleum origin [1-3]. The promising raw materials for the production of biofuel components are triglycerides of fatty acids (non-edible oils, substandard animal fats, food production waste), fatty acid esters and free fatty acids [2-6]. HDO of natural lipids gives normal saturated C_{15}-C_{18} hydrocarbons, which cannot be used as a drop-in paraffinic biofuel (equivalent functionally to petroleum-derived one and compatible with existing infrastructure) without further upgrading because of pour cold flow properties [2-7].

Therefore hydroisomerization/hydrocracking of HDO products (alkanes C_{15}-C_{18}) is required, that gives [4-7]. Hydroprocessed ester and fatty acid (HEFA) is known also as renewable or green diesel, hydrotreated/hydrogenating vegetable oil (HVO), hydrotreated biodiesel. Currently, processes with two catalytic stages are used in industry to obtain paraffinic bio fuel components in diesel, kerosene and gasoline ranges from lipid-based feedstocks, among them NExBTL, UOP/Eni Ecofining™ , UPM BioVerno etc [2,4,6,7]. At the first stage, hydrodeoxygenation of the feedstock is carried out over sulfide catalysts (Ni(Co)Mo/Al_2O_3), at the second stage (after thorough purification from sulfur-containing compounds, CO and CO_2) - hydroisomerization / hydrocracking of the obtained alkanes in the presence of catalysts based on noble metals (Pt on composite carriers, which include zeolites ZSM-22, ZSM-23, SAPO-11).

The development of a one-stage process to obtain paraffinic biofuel component with the appropriate properties in hydroprocessing of lipid-based feedstocks is an urgent task that gets a lot of attention in recent years [6, 8]. The fatty acid methyl ethers (FAME) are often used as a model compound to study the mechanism of reactions and catalytic properties of different materials in hydroconversion of triglycerides. Besides, there is an opinion that it is more profitable to use the product of triglyceride transesterification, fatty acids methyl esters, which makes it possible to obtain value added glycerol in the same process, save hydrogen and reduce the carbon footprint [9-11]. Besides, the hydroconversion of FAME needs a lower reaction temperature and pressure in comparison with triglycerides [6].

It is generally accepted, that unavoidable condition for successive one-step hydroconversion of triglyceride and ethers is the use of a polyfunctional catalyst that ensure the occurrence of several reactions (HDO and hydroisomerization/hydrocracking). According to well-known concept, hydrodeoxygenation of ethers first occurs to form normal alkanes with an even (via direct hydrodeoxygenation route, with the removal of water) or odd (by decarbonylation/decarboxylation) number of carbon atoms [6,8,13]. Hydroisomerization of obtained n-alkanes proceeds via dehydrogenation to alkenes over metallic sites that is protonated by Brønsted acidic sites with carbenium ion formation and subsequent isomerization and hydrogenation [12, 13]. Several articles, dealing with the hydroprocessing of ethers to the mixture of normal and iso-alkane has been reported over bifunctional catalysts, differing in zeolite component and metal function [6,8,14-21].

Pt/SAPO-11 bifunctional catalysts are widely studied in hydroconversion of vegetable oils [6,8,14], the use of Pt/Fe3SAPO-11 showed 100 % conversion of FAME with 99.6 % selectivity to C_{15}-C_{18} alkanes and 34.8 % selectivity of *iso*-C_{15}-C_{18} alkanes with 34.8 % in one-step hydrotreatment at 320, 4 MPa, run time 6 hours in batch reactor [14]. Adding Sn increased the selectivity of *iso*-C_{15}-C_{18} alkanes formation over Pt1Sn1/Fe3SAPO-11 catalyst from 34.8 % to 62.7 %. Despite high activity and selectivity Pt-based catalyst is not preferred in the industrial application because of high cost, low abundance and sensitivity to poison. Hence, the bifunctional catalysts containing transition metals (e.g., Ni, Co) have been tested in FAME hydroprocessing in recent years [15-21].

Ni/HZSM-5 catalysts differing Si/Al ratios and Ni loading was compared in hydroprocessing of long-chain unsaturated fatty acid methyl esters [15]. Selectivity of 88.2% for C_5-C_{18} liquid alkanes was obtained over 10 wt.% Ni/HZSM-5 (Si/Al= 25) at 280°C, 0.8 MPa, LHSV of 4 h^{-1}, and H_2/oil molar ratio of 15, with isomerization selectivity of 27.0%. But conversion of FAME was only 85.1%, that is decreased to 30.1% after operation for 80 h due to carbonaceous deposits. Hydroprocessing of microalgae biodiesel was performed over 10%Ni/meso-Y zeolite catalyst [16], high isomerization ratio (46.4%) and selectivity to jet fuel range hydrocarbons (56.2%) were achieved, but conversion was 91.5% and Ni crystallite size was increased from 25 to 54 nm during hydroprocessing at 275°C and 2.0 MPa. After addition of 4% HPW to 10% Ni/meso-Y catalyst, the production of jet fuel-ranged alkanes and iso-alkane selectivity increased along with increasing of strong acid density [17, 18]. It was shown, that Ni/meso-Y can produce 4,47 % of aromatics, while Ni-based catalysts supported on Meso-ZSM-5, Meso-Hbeta and SAPO-34 tend to produce more aromatics in hydroconversion of microalgae oil in batch reactors at 370-410°c for 8 hours [19]. The Ni-based catalysts are prone to deactivation by coke deposition and agglomeration during the HDO process [15,16,20,21].

The comparison of Ni/SAPO-11, Co/SAPO-11 and NiCo/SAPO-11 in hydroconversion of FAME were performed at 360-440°C, 1.5 MPa and WHSV of 2.6 $hours^{-1}$ [20]. Ni-Co/SAPO-11 catalyst, containing 3% Ni and 6% Co exhibited the optimal catalytic properties, providing 100.0%, conversion of FAMEs, 93.0% selectivity to C_{15}-C_{18} hydrocarbons and 36.1% of isomerization ratio at 400°C.

Ni/SAPO-11 and Ni_2P/SAPO-11 catalysts were compared in hydroconversion of methyl laurate (ML) at 320-380°C, 1.0-5.0 MPa, WHSV of 2-8 h^{-1}, and H_2/ML molar ratio of 25 [21]. Ni_2P/SAPO-11 exhibited higher stability in comparison to Ni/SAPO-11 in HDO of ML, but both catalysts lost hydroisomerization activity. The ML conversion was close to 100% at 360 °C, 3.0 MPa, WHSV of 2 h^{-1} while selectivity to *iso*-undecane and *iso*-dodecane decreased from 36.9% to 28.6% on Ni_2P/SAPO-11 for 100 hours. It was shown, that sintering of Ni particles and formation of carbonaceous deposit was observed on spent Ni/SAPO-11, while no obvious increase of Ni_2P particles took place and carbonaceous deposit was a reason to deactivation hydroisomerization activity of Ni_2P/SAPO-11 [21].

Sulfided NiMo/SAPO-11 and NiMo/AlSBA-15 catalysts were studied in the hydroconversion of methyl stearate at 300–375°C, 3 MPa, LHSV of 10 h^{-1}, and volume H_2/feed ratio of 600 [13]. Both NiMo

Preprints (www.preprints.org) | NOT PEER-REVIEWED | Posted: 19 September 2023 doi:10.20944/preprints202309.1239.v1

catalysts provided high HDO conversion (above 99%) and isomerization activities, but NiMo/SAPO-11 exhibited higher yield of iso-alkanes, while NiMo/AlSBA-15 catalysts promoted additionally the formation of cracked products. The authors conclude, that moderate acidity and a suitable pore size of SAPO-11 provide formation of mono-branched isomers.

The efficiency of unpromoted sulfide MoS_2 was demonstrated recently in MP hydrodeoxygenation [22], wherein alumina-supported MoS_2 demonstrate high selectivity for the conversion of aliphatic ethers through the direct HDO route, without the formation of carbon oxides [23-25]. This property allows to avoid effect of carbon oxides on the catalyst lifetime and additional purification of the recycle gas from CO_x [26]. To the best of our knowledge, the activity of MoS_2 nanoparticles dispersed on zeolite-containing supports has not been studied yet in the hydroprocessing of aliphatic ethers.

The purpose of this work is the comparative study of sulfide Mo-containing catalysts supported on granulated composite supports differing in the nature of the zeolite (Al_2O_3-ZSM-5, Al_2O_3-ZSM-12, Al_2O_3-SAPO-11, Al_2O_3-ZSM-22), in the hydroprocessing of methyl palmitate. The MoS_2/Al_2O_3-Z catalysts have been prepared with the use of organic additives ensuring the high dispersion of MoS_2 nanoparticles after proper sulfidation with DMDS/dodecane solution. Characterization has been performed using wide set of different techniques to compare the MoS_2 size/location and the acidity of support depending on zeolite and to elucidate the possible correlations between physico-chemical and catalytic properties.

3. Results and Discussion

3.1. Catalyst characterization

Textural properties of the synthesized supports and Mo content in the catalysts listed in Table 1. All supports had similar textural properties: surface area – about 170 m^2/g, pore volume – about 0.5 cm^3/g and pore diameter – above 20 nm. The prepared catalysts contained about 7.0 wt.% of molybdenum. Such Mo concentration was chosen to get monolayer on support surface (4.0 at Mo/nm^2) [27]. Wherein it was taken into account that MoS_2 localized predominantly on alumina surface.

Table 1. The properties of the prepared catalysts.

Catalysts	Mo, wt.%	Support	Textural properties of the support		
			Surface area, m^2/g	Pore volume, cm^3/g	Pore diameter, nm
Mo/Al_2O_3	6.95	Al_2O_3	133	0.66	25.1
Mo/Al_2O_3-ZSM-5	6.90	Al_2O_3-ZSM-5	202	0.48	25.6
Mo/ Al_2O_3-ZSM-12	6.96	Al_2O_3-ZSM-12	165	0.49	22.8
Mo/ Al_2O_3-ZSM-22	6.90	Al_2O_3-ZSM-22	175	0.53	25.5
Mo/ Al_2O_3-SAPO-11	6.97	Al_2O_3-SAPO-11	177	0.42	22.6

According to XRD data of synthesized supports the alumina and corresponding zeolite diffraction lines were clearly observed (Figure 1). The supports contained a nanocrystalline alumina phase of γ-Al_2O_3 (PDF № 00-029-0063, the cubic cell parameter was a= 7.915 Å, the determined average size of coherently scattering domain was 7.5 nm) and corresponding crystalline phase of zeolite ZSM-5 (PDF# 00-044-0003, the determined average size of coherently scattering domain was 80 nm), ZSM-12 (PDF# 00-086-2634 a=24.863 Å, b=5.012 Å, c=24.372 Å β=107.7^0, the determined average size of coherently scattering domain was 45 nm), ZSM-22 (PDF# 00-038-0197 a=13.83 Å, b=17.41 Å, c=5.042 Å, the determined average size of coherently scattering domain was 45 nm) and silicoaluminophosphate SAPO-11 $Al_2Si_{0.35}P_{1.74}O_{8.05}$ (PDF# 00-047-0614, the determined average size of coherently scattering domain was 70 nm).

Preprints (www.preprints.org) | NOT PEER-REVIEWED | Posted: 19 September 2023 doi:10.20944/preprints202309.1239.v1

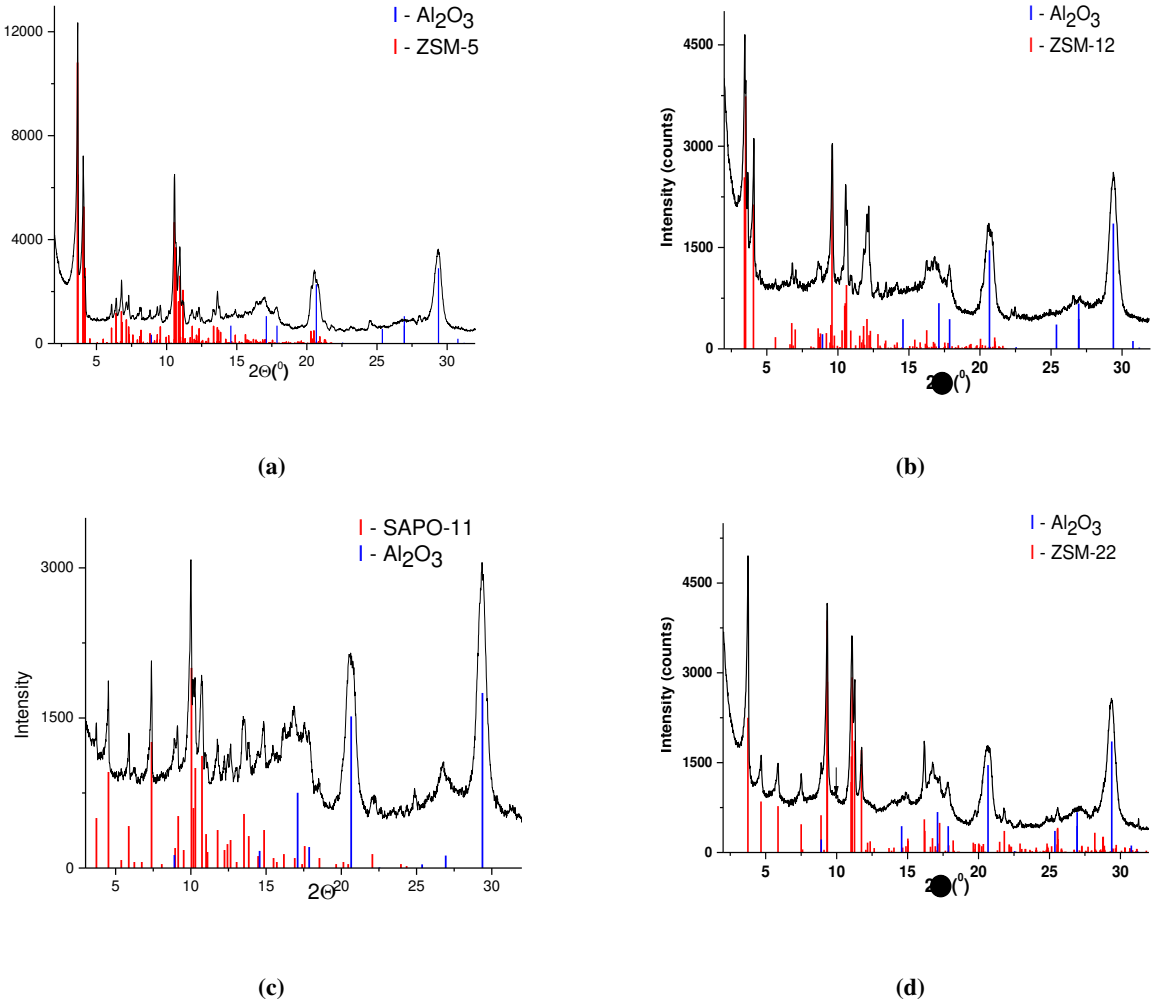

Figure 1. XRD patterns of synthesized Al_2O_3-zeolite composite supports (**(a)** – Al_2O_3-ZSM-5, **(b)** – Al_2O_3-ZSM-12, **(c)** – Al_2O_3-SAPO-11, **(d)** – Al_2O_3-ZSM-22).

SEM pictures of zeolite materials and final supports Al_2O_3-zeolite are shown in Figure 2. Zeolite fragments presented on SEM images of composite supports evidence to preservation of zeolite structure in synthesized supports Al_2O_3-zeolite. Moreover, EDX mapping of Al_2O_3-zeolite supports demonstrates uniform distribution of zeolite in support granules. Zeolites in the synthesized supports Al_2O_3-zeolite display different average particle sizes (930, 1010, 300 and 220 nm for ZSM-5, ZSM-12, SAPO-11 and ZSM-22), and their histograms of particle size distribution are given in Figure 3 (the scale was chosen so that ethe difference was visually seen).

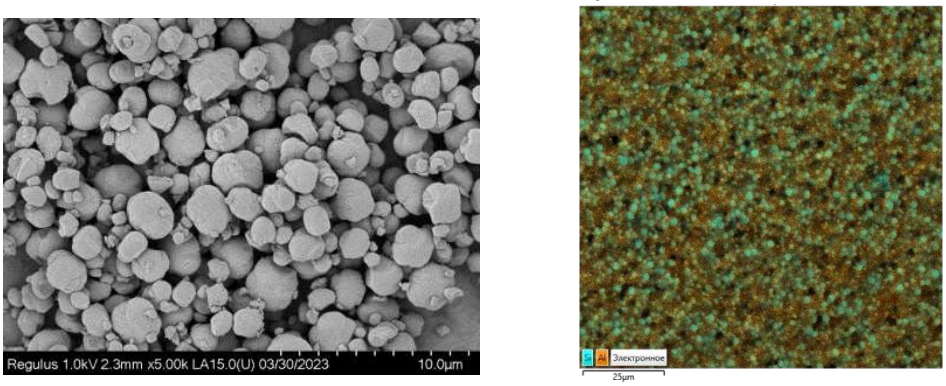

ZSM-5 Al_2O_3-ZSM-5

Preprints (www.preprints.org) | NOT PEER-REVIEWED | Posted: 19 September 2023 doi:10.20944/preprints202309.1239.v1

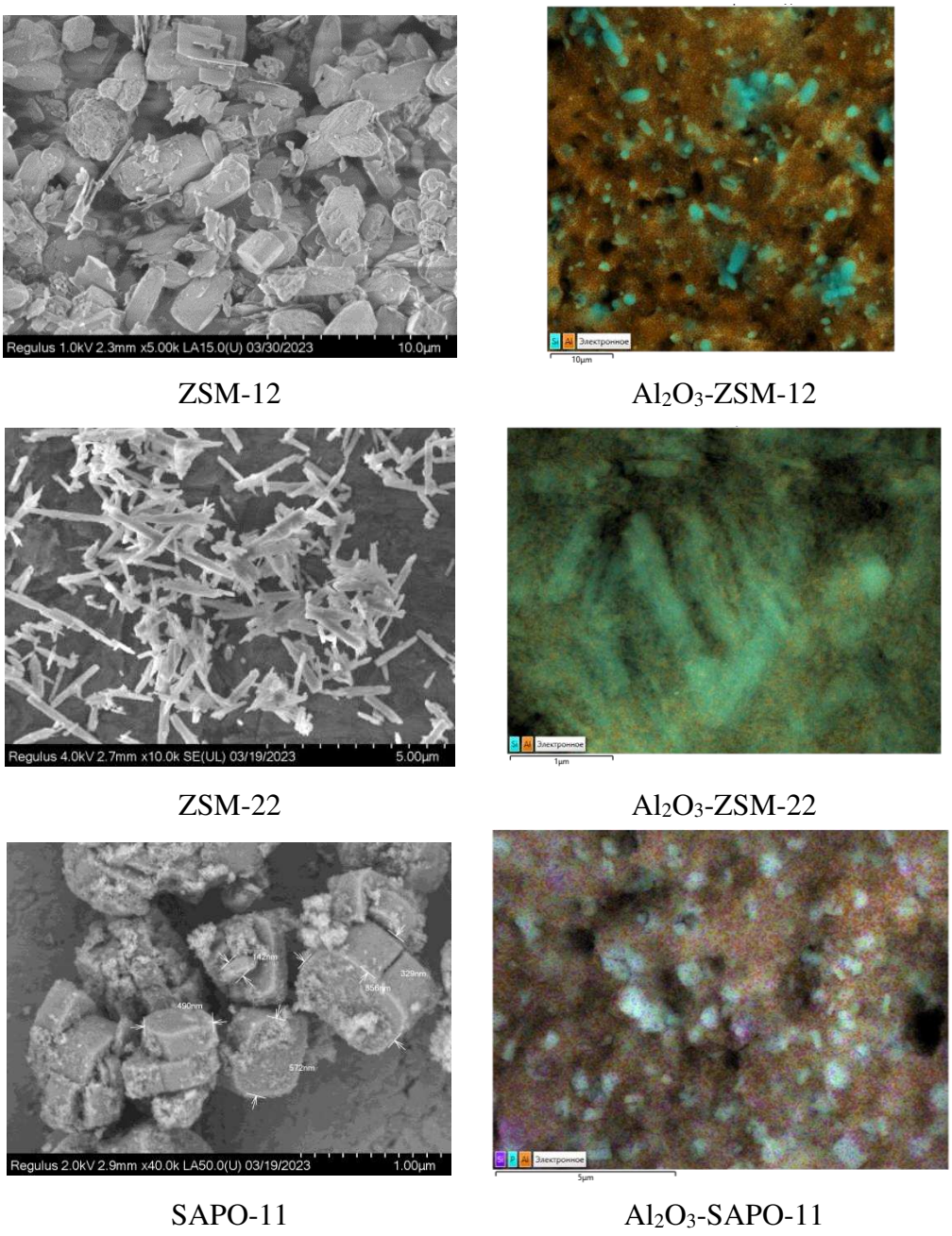

Figure 2. SEM images of zeolite material (left) and EDX maps of composite supports Al_2O_3-zeolite (right).

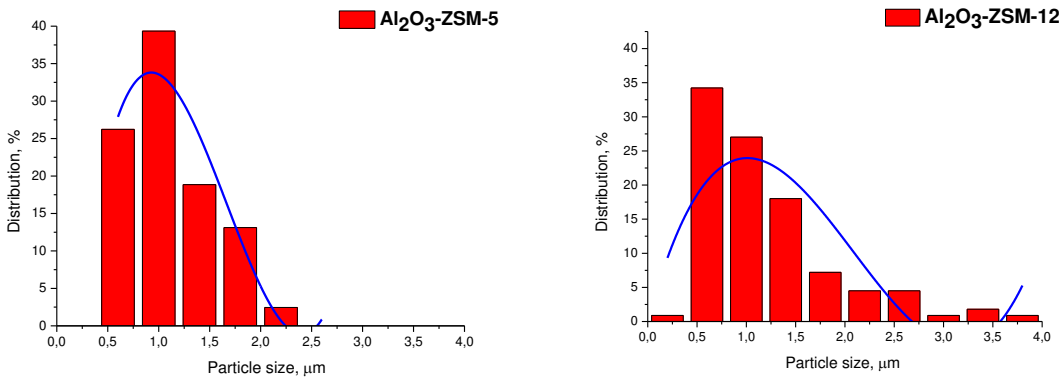

Preprints (www.preprints.org) | NOT PEER-REVIEWED | Posted: 19 September 2023 doi:10.20944/preprints202309.1239.v1

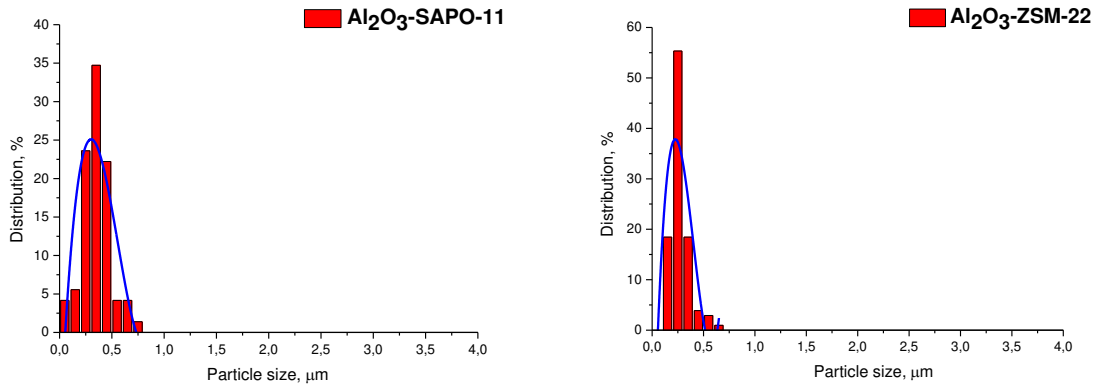

Figure 3. Histograms of zeolite particle size distribution for supports Al_2O_3-zeolite (a) Al_2O_3-ZSM-5 (average particle size 930 nm), (b) Al_2O_3-ZSM-12 (average particle size 1010 nm), (c) Al_2O_3-SAPO-11 (average particle size 300 nm), and (d) Al_2O_3-ZSM-22 (average particle size 220 nm).

The hydroxyl cover of Al_2O_3 and Al_2O_3-zeolite supports was studied by FTIR spectroscopy (Figure 4). The spectrum of pure alumina shows the vibration bands at *ca.* 3790, 3775, 3727, 3700–3685 and 3660 cm^{-1}, which are typical for FTIR spectrum of surface OH groups of γ-Al_2O_3 [28] and characterized the different type of the terminal Al-OH and bridged Al–O(H)-Al groups. The spectra of alumina-zeolite composites present two groups of signals in the region of O-H stretching vibrations assigned to the hydroxyl groups of the zeolites and the alumina binder. The intensity of bands at 3790, 3770, 3727 and 3685-3700 cm^{-1} in the spectra of composites (except for the Al_2O_3-SAPO-11) is proportional to the binder content. In the spectrum of Al_2O_3-SAPO-11 sample, a decrease in the intensity of the bands of binder hydroxyl is observed, possibly caused by the interaction of phosphate ions from SAPO-11 both with Al-OH and Al-O(H)-Al groups of alumina. The signal at 3676 cm^{-1} in the spectrum of this composite characterize P-OH groups either in the structure of PO_4 tetrahedron at the external surface of silica aluminophosphates [29] or at the surface of PO_4-doped alumina [30]. The framework Si-O(H)-Al groups of SAPO-11, corresponding to strong Brønsted acid sites (BAS), appear at 3628 cm^{-1} for Al_2O_3-SAPO-11 composite in accordance with [29] at 3602 cm^{-1} for Al_2O_3-ZSM-22 [31], at 3612 cm^{-1} for Al_2O_3-ZSM-5 [32] and at 3612 and 3575 cm^{-1} for Al_2O_3-ZSM-12 composites [33]. The intensity of the bands of bridged hydroxyls in zeolite channels for Al_2O_3-ZSM-5 and Al_2O_3-ZSM-22 composites is significantly higher than for Al_2O_3-ZSM-12 and Al_2O_3-SAPO-11 ones. The bands of hydroxyl groups attached to partially extra-framework Al-OH species of zeolites overlap with the peaks of bridged Al–O(H)-Al groups of Al_2O_3. The bands at 3745 and 3738-3740 cm^{-1} in the spectra of Al_2O_3-zeolite extrudates are assigned to terminal silanols and defect Si-OH groups located in the close vicinity to the lattice imperfection or Lewis acid sites at the external surfaces of zeolite crystals [34], respectively.

Preprints (www.preprints.org) | NOT PEER-REVIEWED | Posted: 19 September 2023 doi:10.20944/preprints202309.1239.v1

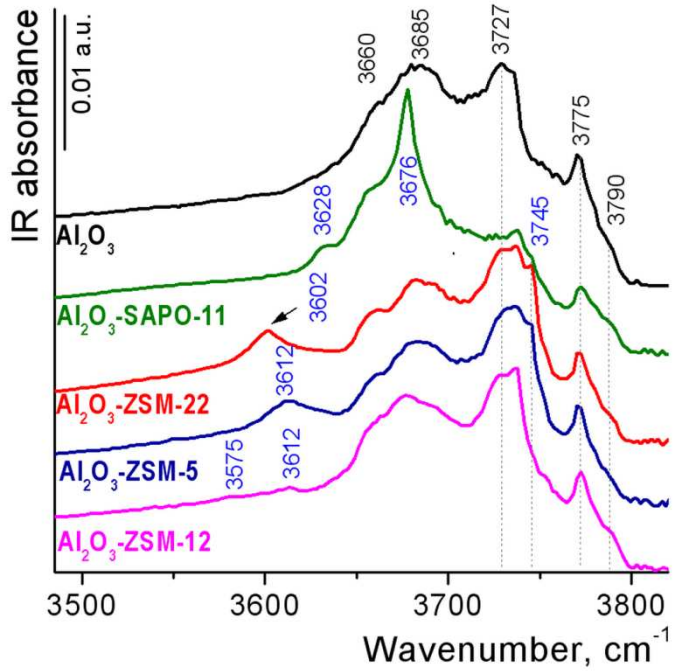

Figure 4. FTIR spectra of Al_2O_3 and Al_2O_3-zeolite supports after outgassing at 500°C in the O-H stretching region.

Acid properties of the Al_2O_3-zeolite supports were studied by FTIR spectroscopy with progressive CO adsorption at liquid nitrogen temperature. Adsorption of CO on pure Al_2O_3 at low pressures (spectra not shown) leads to the appearance of bands at 2241, 2235, 2220-2218 and 2208-2206 cm^{-1}, assigned to the coordinately bonded CO complexes with strong and moderate Lewis acid sites (LAS) [35]. An increase in CO pressure leads to the appearance of a band at about 2200 cm^{-1}, red shifted to 2184-2186 cm^{-1} at increasing coverage, which attributed to the CO complex with weak LAS of alumina. The signals at 2164 and 2158-2156 cm^{-1} indicate CO complex with different type of Al–OH groups. The spectra of CO adsorbed on Al_2O_3-zeolite supports presents bands related to CO adsorption both on pure alumina and on zeolites (Figure 5). The bands at 2225-2230 cm^{-1}, which are attributed to the complexes of CO with strong LAS of zeolites, overlap with the same bands of CO complex with Al_2O_3 species. The concentration of strong and moderate LAS in Al_2O_3-zeolite composites varies insignificantly (except Al_2O_3-SAPO-11); the amount of weak LAS is the same and proportional to the alumina content in the composites. An increase in the concentration of moderate LAS with the band at 2206 cm^{-1}, apparently related to Al^{3+} species modified by PO_4^{2-} groups [30], is observed for the Al_2O_3-SAPO-11 support (Figure S1 in the Supplementary Materials)

The spectra of Al_2O_3-zeolite samples demonstrate additional signals at 2178-2170 and 2137-2138 cm^{-1} at the CO stretching region compared to the spectra of pure alumina. The first group of bands refers to CO complexes with BAS, the second peak characterizes physically or liquid-like adsorbed CO molecules in zeolite channels [32]. The spectra of Al_2O_3-ZSM-5 and Al_2O_3-ZSM-22 supports exhibit one signal for CO complexes with strong BAS at 2176 cm^{-1}, which corresponds to the spectra of pure zeolites [36-38]. The spectra of Al_2O_3-SAPO-11 composite present one band for CO complexes with BAS at 2173 cm^{-1}, red shifted to 2170 cm^{-1} at increasing coverage, which corresponds to moderate BAS in accordance with the value of CO-induced blue shift relative the CO gas phase ($\Delta\nu_{CO}$ = 30-27 cm^{-1}). The band at 2178 cm^{-1} in the spectra of Al_2O_3-ZSM-12 support is assigned to CO complex with strong BAS, while the signal at 2171 cm^{-1} belongs to CO complex with moderate BAS. Two types of BAS, framework Si-O(H)-Al groups and extra-framework Al-OH groups, are also observed in the spectra of the original ZSM-12 zeolite [33]. The CO complex with Na^+ impurities in the ZSM-12 zeolite additionally increases the intensity of the band at 2171–2170 cm^{-1} in case of Al_2O_3-ZSM-12 composite.

Preprints (www.preprints.org) | NOT PEER-REVIEWED | Posted: 19 September 2023 doi:10.20944/preprints202309.1239.v1

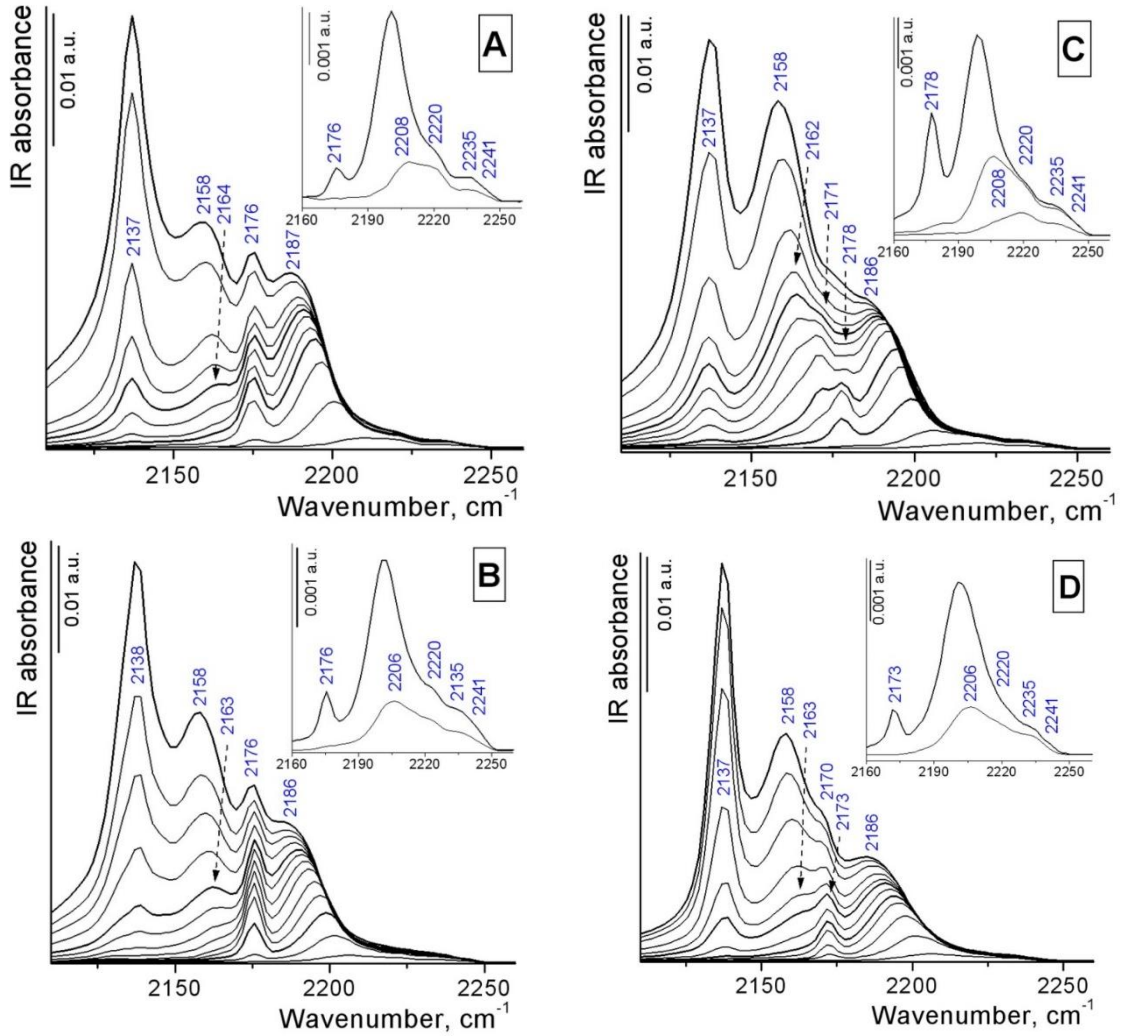

Figure 5. FTIR spectra of CO adsorbed at liquid nitrogen temperature on Al_2O_3-zeolite supports: Al_2O_3-ZSM-5 (A), Al_2O_3-ZSM-22 (B), Al_2O_3-ZSM-12 (C), Al_2O_3-SAPO-11 (D). Equilibrium CO pressures used were from 0.1 (bottom curve) to 5 mbar (top curve). The inset show enlarged spectra at low CO pressure. All spectra are background corrected.

The weakly basic CO molecule is known to be a good probe molecule for testing the strength of BAS in zeolites and related materials [39]. During low-temperature CO adsorption on Al_2O_3-zeolite samples, the bands of acidic OH groups fully disappeared, and a new band appeared (Figure 6). The red-shift of OH stretching vibration at hydrogen bonding with carbon monoxide is traditionally used to estimate the acidity of hydroxyl groups. A new positive peak at about 3285 and 3300 cm^{-1} appears in the spectra of Al_2O_3-ZSM-22 and Al_2O_3-ZSM-5 samples, respectively, at low CO pressure. The value of red frequency shift of the bands from the framework Si-O(H)-Al groups at hydrogen bonding with CO ($\Delta\nu_{OH...CO}$) is 317-320 cm^{-1} and similar to the magnitude for initial zeolites [36-38]. The corresponding blue frequency shift of the CO stretching bands for these composites is also the same ($\Delta\nu_{CO}$ = 33 cm^{-1}), which indicates a similar high acidity of the bridged hydroxyls. Quantitative data on BAS concentration and acid strength are given in the Table 3. A large concentration of strong BAS for the Al_2O_3-ZSM-22 composite is obviously associated with a lower Si/Al ratio in the structure of the zeolite used. The shoulder at about 3400 cm^{-1} in the spectra of Al_2O_3-ZSM-5 and Al_2O_3-ZSM-22 supports changing in synchrony with the band at 3285-3300 cm^{-1} is due to Fermi resonance [40]. Other positive bands are appeared at 3470-3480 cm^{-1} in the spectra of these composite and related to hydrogen bonded CO complex with defect silanol groups (Si-O(H)…Al^{3+}). The shift value ($\Delta\nu_{OH...CO}$ = 270-260 cm^{-1}) are slightly lower than the magnitude typical for bridged Si-O(H)-Al groups in the zeolite channel and correspond to moderately strong BAS. The concentration of these sites is negligible.

Preprints (www.preprints.org) | NOT PEER-REVIEWED | Posted: 19 September 2023 doi:10.20944/preprints202309.1239.v1

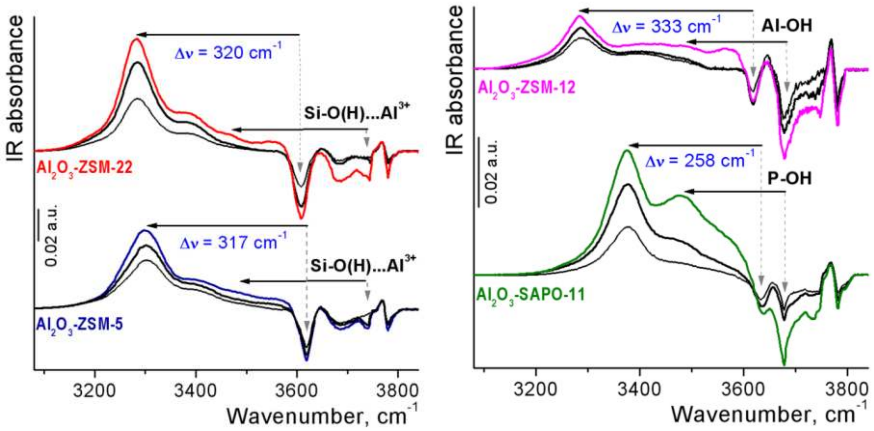

Figure 6. FTIR difference spectra of the OH stretching region during adsorption of CO on Al2O3-zeolite supports at liquid nitrogen temperature and low equilibrium CO pressure of 0.3, 0.5 and 1 mbar.

After CO adsorption on Al_2O_3-ZSM-12 sample the appearance of the new positive signal at 3285 cm^{-1} is observed. The values of red frequency shift in hydroxyl region ($\Delta\nu_{OH...CO}$ = 333 cm^{-1}) and corresponding blue frequency shift in carbonyl region ($\Delta\nu_{CO}$ = 35 cm^{-1}) in the spectra of this support is assigned to BAS with enhanced acidity that bridged hydroxyl in the zeolite channel for Al_2O_3-ZSM-22 and Al_2O_3-ZSM-5 composites. The magnitude of shifts is slightly higher than in pure zeolite [33]. The low concentration of strong BAS for the Al_2O_3-ZSM-12 composite compared to the Al_2O_3-ZSM-5 composite may be due to their partial exchange with Na^+ impurity. Other band in the O–H stretching region after CO adsorption on the Al_2O_3-ZSM-12 composite detects at ~ 3460–3490 cm^{-1} and related to perturbation both of extra-framework Al-OH groups of zeolite with the band at about 3670-3675 cm^{-1} and the defect silanols with the band at 3738-3740 cm^{-1}. Apparently, ZSM-12 zeolite is partially dealuminated. According to the values red frequency shift, the extra-framework Al-OH groups in this zeolite is BAS with medium strength. Progressive CO adsorption on Al_2O_3-SAPO-11 composite leads to appearance strong positive band at the 3378 cm^{-1} with the shoulder at 3470 cm^{-1} due to perturbation of bridged Si-O(H)-Al groups in the zeolite channels. The shift value ($\Delta\nu_{OH...CO}$ = 258 cm^{-1}) is significantly lower than the magnitude typical for bridged Si-O(H)-Al groups in the pure SAPO-11 channel ($\Delta\nu_{OH...CO}$ = 310 cm^{-1}) [41] and correspond to moderately strong BAS. The change in the acidity of bridged Si-O(H)-Al groups in the zeolite channels can be probably caused by disruption of the SAPO-11 structure by the partial removal of phosphate groups during molding of extrudates. The red shift of P-OH groups of zeolites after CO adsorption ($\Delta\nu_{OH...CO}$ = 202÷198 cm^{-1}) correspond to somewhat weaker Brønsted acid sites.

Thus, the strength of framework BAS (bridged Si-O(H)-Al groups in zeolite channels) decreases in the series of Al_2O_3-zeolite supports as Al_2O_3-ZSM-12 > Al_2O_3-ZSM-22 ~ Al_2O_3-ZSM-5 >> Al_2O_3-SAPO-11, while the concentration of strong and moderate BAS of zeolites decreases in the following order: Al_2O_3-ZSM-22 > Al_2O_3-SAPO-11 > Al_2O_3-ZSM-5 >> Al_2O_3- ZSM-12.

In FTIR difference spectra during adsorption of CO on pure alumina, there are no bands in the region of 3200-3500 cm^{-1} [42] which are characteristic of CO complexes with BAS of zeolites. The terminal Al-OH groups of alumina are traditionally assigned basic properties, while the bridging hydroxyls have been shown to have weak acidic properties ($\Delta\nu_{OH...CO}$ = 130÷100 cm^{-1}). The formation of CO complexes with the Al-O(H)-Al groups of alumina during CO adsorption on Al_2O_3-zeolite supports occurs after saturation of the zeolite BAS (Figure S2 in the Supplementary Materials).

Table 3. Type, acid strength and concentration of Brønsted acid sites of Al_2O_3-zeolite composite supports.

Al_2O_3-zeolite composites	Type of zeolite sites	IR frequency shift / cm^{-1}		BAS concentration (μmol g^{-1})
		$\Delta\nu_{OH...CO}$[a]	$\Delta\nu_{CO}$[b]	
Al_2O_3-ZSM-5	Framework Si-O(H)-Al groups	–317	+33	8.1

Preprints (www.preprints.org) | NOT PEER-REVIEWED | Posted: 19 September 2023 doi:10.20944/preprints202309.1239.v1

	Extra-framework Si-O(H)…Al^{3+} groups	–(260÷270)		1.8
Al_2O_3-ZSM-22	Framework Si-O(H)-Al groups	–320		11.4
	Extra-framework Si-O(H)…Al^{3+} groups	–(260÷270)	+33	1.0
Al_2O_3-ZSM-12	Framework Si-O(H)-Al groups	–333	+35	2.7
	Extra-framework Al-OH groups	–(200÷196)	+28	2.6
Al_2O_3-SAPO-11	Framework Si-O(H)-Al groups	–258	+30	7.4
	P-OH groups	–(202÷198)	+27	~4[c]

[a] Red frequency shift of the bands of O-H groups at hydrogen bonding with CO. [b] Blue frequency shift of the CO stretching bands at hydrogen bonding of CO with OH- groups relative the gas phase CO. [b] The contribution of the P-OH groups for the SAPO-11 is approximate (molar integral absorption coefficients for P-OH group unknown).

According to HRTEM images (Figure 7) dispersed sulfide phase is presented on the surfaces of the sulfided catalysts which is visualized as a black line (edges of MoS_2 particles). The average size of nanoparticles was varied from 4 to 6 nm; stacking number was 1.5-1.7 for all catalysts. It should be noted that MoS_2 nanoparticles were predominantly located on the alumina surface and only single species presented on surface of zeolite, this statement is illustrated for MoS_2/Al_2O_3-SAPO-11 and MoS_2/Al_2O_3-ZSM-22 catalysts on Figure 7. EDX mapping confirms this statement: sulfide species (Figure 8, green color) are more prevalent on alumina surface in comparison with zeolite surface (Figure 8, red color) where sulfide particles far less.

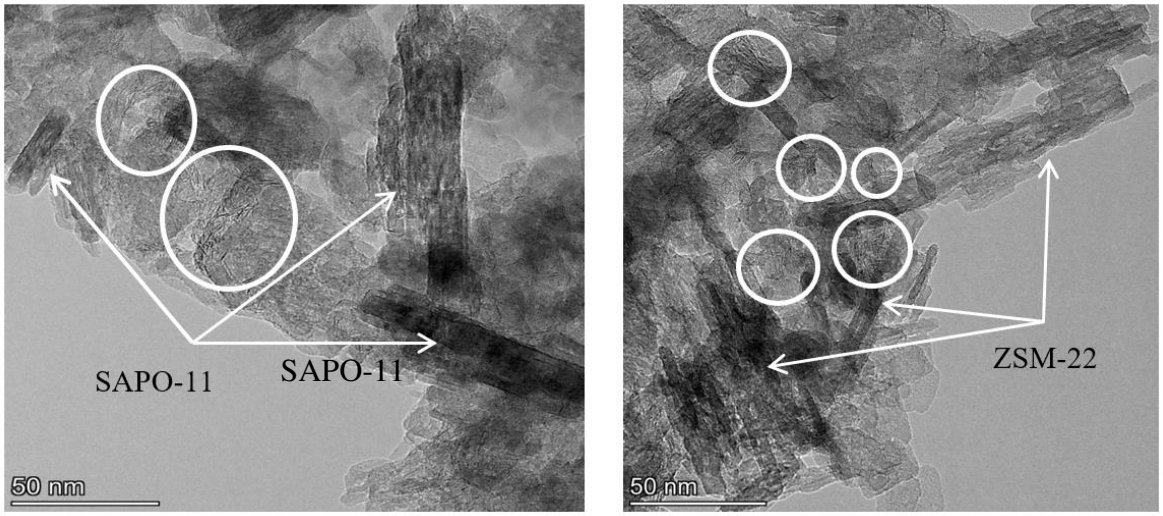

Figure 7. HRTEM images of MoS_2/Al_2O_3-SAPO-11 and MoS_2/Al_2O_3-ZSM-22 catalysts (curcle – sulfide nanoparticles on alumina surface).

Preprints (www.preprints.org) | NOT PEER-REVIEWED | Posted: 19 September 2023 doi:10.20944/preprints202309.1239.v1

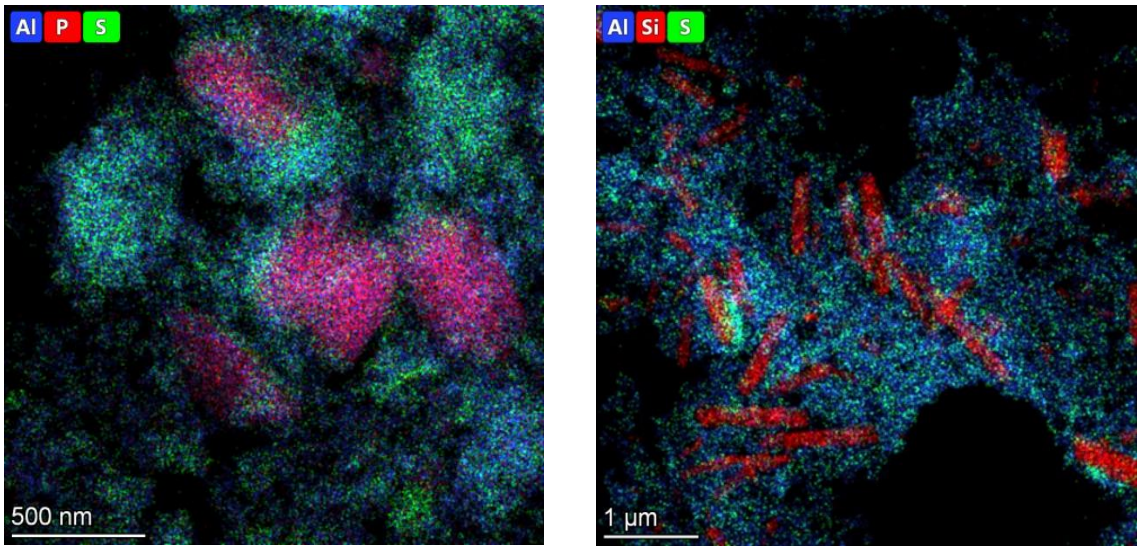

Figure 8. HRTEM-EDX mapping of MoS_2/Al_2O_3-SAPO-11 and MoS_2/Al_2O_3-ZSM-22 catalysts.

3.2. The effect of zeolite type on hydrodeoxygenation of methyl palmitate

The conversion of fatty acid esters can follow through two routes: 'direct' hydrodeoxygenation ('direct' HDO) and hydrodecarboxylation/hydrodecarbonylation (DeCOx). In the presence of MoS_2 catalyst the conversion of fatty acid esters proceeded mainly via a 'direct' hydrodeoxygenation pathway to form hexadecane ($C_{16}H_{34}$) and water with formation of carbon oxides only in trace amounts [24,43,44].

Hydrodeoxygenation (HDO) of methyl palmitate (MP) was performed at temperature range of 250-350°C, at H_2 pressure 3.0 MPa, H_2/feed ratio – 600 Nm^3/m^3 and LHSV – 36 h^{-1}. Methyl palmitate conversion is increased with the temperature rising from 250 to 310°C (Figure 9). Hexadecanol, hexadecanal, palmitic acid, palmityl palmitate and methyl hexadecyl either were detected as oxygen intermediate products over MoS_2/Al_2O_3-zeolite catalysts in MP hydrodeoxygenation, in consistence with the previous results [22, 23, 45]. At temperature range 250-290°C normal and unsaturated C_{15}-C_{16} alkanes were also observed.

Figure 9 shows that the addition of zeolite to alumina has slight influence on MP conversion. Conversions of all-oxygen-containing compounds including both intermediates and methyl palmitate were calculated using the contents of oxygen in the reaction mixture before and after reaction by means of elemental analysis (Eq. 1-2) and the results are presented on Figure 10. According to these results, the addition of zeolite to the support leads to an increase in the conversion of oxygen-containing compounds. Taking into account that the conversion of methyl palmitate weakly depends on the composition of the carrier, we can conclude that the addition of zeolite leads to an acceleration of the HDO reactions of intermediate oxygen-containing compounds [13].

Complete MP and oxygen conversion was achieved at 310°C in the presence of all catalysts (Figures 9-10). Normal and iso-alkanes (C_{15} and C_{16}) were detected under conditions when complete oxygen conversion was achieved (at temperature above 310°C). Cracked products were detected in negligible amounts over MoS_2/Al_2O_3-SAPO-11 and MoS_2/Al_2O_3-ZSM-22 catalysts: 2 and 4% at temperature 350°C, respectively. The maximum of cracked products yield was observed for MoS_2/Al_2O_3-ZSM-5 (18%) and MoS_2/Al_2O_3-ZSM-12 (12%) catalysts.

The selectivity for the conversion of methyl palmitate via the 'direct' hydrodeoxygenation route in the presence of MoS_2/Al_2O_3-zeolite catalysts was over 85% (Figure11). Temperature increase leads to a decrease in the selectivity of the $C_{16}H_{34}$ formation via 'direct' HDO route over all catalysts due to occurring DeCOx reactions (Figure 11) [46]. It can be seen that addition of zeolite into alumina resulted in enhance of DeCOx route in hydroprocessing of MP over sulfide catalysts (Figure 11). The lowest HDO selectivity was observed over MoS_2/Al_2O_3-ZSM-22 catalyst. It can be explained by the highest concentration of strong BAS on Al_2O_3-ZSM-22 support surface (Table 3) that could favor hydrodecarboxylation/ hydrodecarbonylation reactions of methyl palmitate. Methane and negligible amounts of carbon monoxide were detected in gas phase.

Preprints (www.preprints.org) | NOT PEER-REVIEWED | Posted: 19 September 2023 doi:10.20944/preprints202309.1239.v1

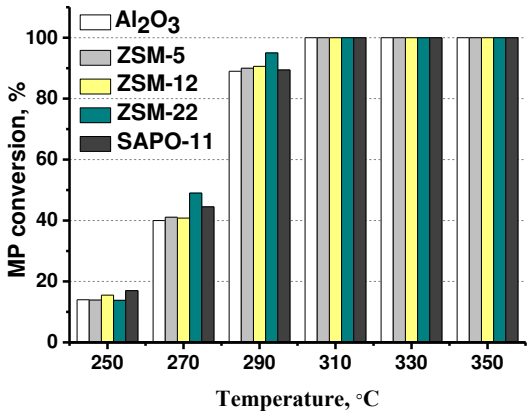

Figure 9. MP conversion in dependence on temperature over MoS_2/Al_2O_3-zeolite catalysts. (reaction conditions: 250-350°C, 3.0 MPa, 600 Nm^3/ m^3, 36 h^{-1}).

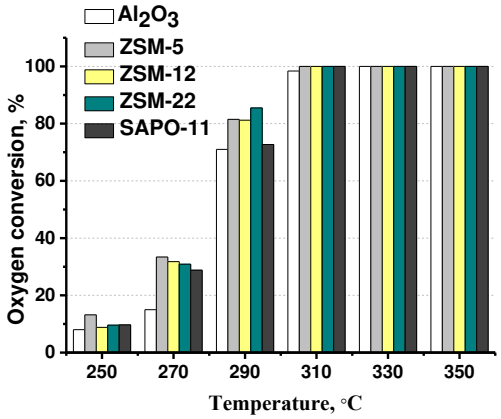

Figure 10. The conversion of oxygen-containing compounds in dependence on temperature over MoS_2/Al_2O_3-zeolite catalysts (reaction conditions: 250-350°C, 3.0 MPa, 600 Nm^3/ m^3, 36 h^{-1}).

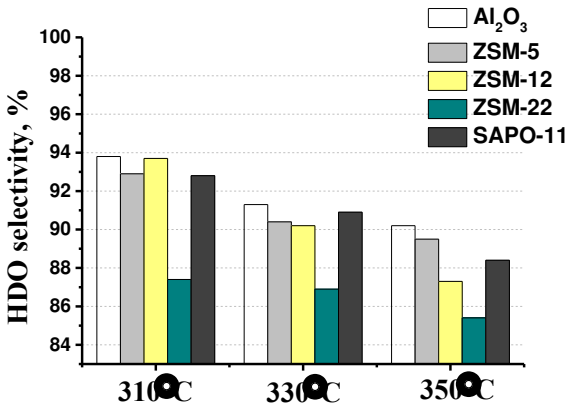

Figure 11. Temperature effect on HDO selectivity over MoS_2/Al_2O_3-zeolite catalysts (reaction conditions: 310-350°C, 3.0 MPa, 600 Nm^3/ m^3, 36 h^{-1}).

The catalyst stability in hydrodeoxygenation of methyl palmitate was checked after 40 hours at temperature 290°C. Oxygen conversion was changed slightly: from 81.5 to 80.0% for MoS_2/Al_2O_3-ZSM-5, from 81.2 to 77.0% for MoS_2/Al_2O_3-ZSM-12, from 85.5 to 82.9 for MoS_2/Al_2O_3-ZSM-22 and from 72.7 to 68.0% for MoS_2/Al_2O_3-SAPO-11. Thus, the change in catalyst activity during the experiment can be neglected.

Preprints (www.preprints.org) | NOT PEER-REVIEWED | Posted: 19 September 2023 doi:10.20944/preprints202309.1239.v1

3.3. The effect of zeolite type on hydroisomerization of methyl palmitate

The isomerization process over MoS_2/Al_2O_3-zeolite catalysts was studied under the conditions of complete conversion of oxygenates, i.e., temperature above 310°C, and pressure 3.0 and 5.0 MPa. The catalytic activity of the sulfide samples during the hydroisomerization of methyl palmitate was compared by the yield of isomeric $C_{16}H_{34}$ and $C_{15}H_{32}$ alkanes in the reaction products.

According to the obtained results the yield of iso-alkanes gradually increases in order: MoS_2/Al_2O_3<MoS_2/Al_2O_3-ZSM-12<MoS_2/Al_2O_3-ZSM-5<MoS_2/Al_2O_3-SAPO-11< MoS_2/Al_2O_3-ZSM-22: yield of iso-alkanes did not exceed 5% over MoS_2/Al_2O_3, 13.5% and 7.4% for MoS_2/Al_2O_3-ZSM-5 and MoS_2/Al_2O_3-ZSM-12 samples, accordingly at 310°C, 3.0 MPa, 600 Nm^3/m^3, 36 h^{-1}. In the presence of MoS_2/Al_2O_3-SAPO-11 catalyst, the yield of iso-alkanes increases to 24%, the most active catalyst in the MP hydroisomerization was the MoS_2/Al_2O_3-ZSM-22 with a yield of isomerized $C_{16}H_{34}$ and $C_{15}H_{32}$ alkanes of 40% (Figure 12). Observed sequence coincides with the increase of the BAS concentration order of zeolite-containing supports: Al_2O_3-ZSM-12 << Al_2O_3-ZSM-5 < Al_2O_3-SAPO-11 Al_2O_3-ZSM-22. Hydroisomerization activity of sulfide catalysts is proportional to the number of BAS [13, 47].

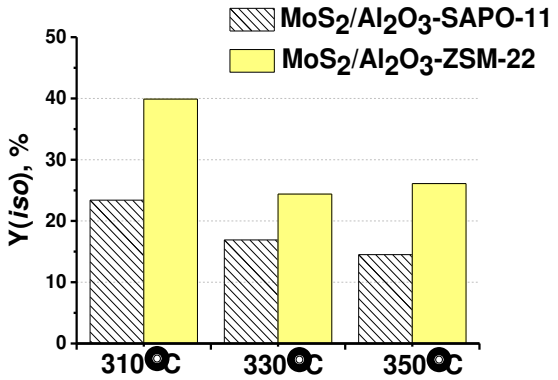

Figure 12. Temperature effect on yield of isomeric $C_{16}H_{34}$ and $C_{15}H_{32}$ alkanes over MoS_2/Al_2O_3-SAPO-11 and MoS_2/Al_2O_3-ZSM-22 catalysts (reaction conditions: 310-350°C, 3.0 MPa, 600 Nm^3/m^3, 36 h^{-1}).

It was observed that catalytic properties depend not only on acidity of samples but also on pore structure and framework topology of zeolites in the catalyst's composition [48]. MP molecule has a length of 22 Å and a width of 2.2 Å (Figure 13). According to the literature data to isomerize MP molecule should be available to diffuse into pores and channels of zeolite [13]. Catalytic experiments showed that catalysts prepared with ZSM-22 and SAPO-11 demonstrated a better performance in hydroisomerization of methyl palmitate. It is correlated with BAS concentration of synthesized zeolite-containing supports. Moreover, better performance of ZSM-22- and SAPO-11-containing catalysts probably could be explained by smaller average crystallite size of zeolite in comparison with catalysts prepared with ZSM-5 and ZSM-12 (Figure 3). We can propose, that zeolite with smaller crystallite size gives more uniform (homogeneous) distribution in the support, that in turn provides closer proximity of zeolite and sulfide entities. There is no consensus in literature data about influence of zeolite particle size on efficiency of zeolite-containing catalysts in hydroprocessing [49-53]. Probably acidity is more significant factor than pore structure and framework topology of zeolites.

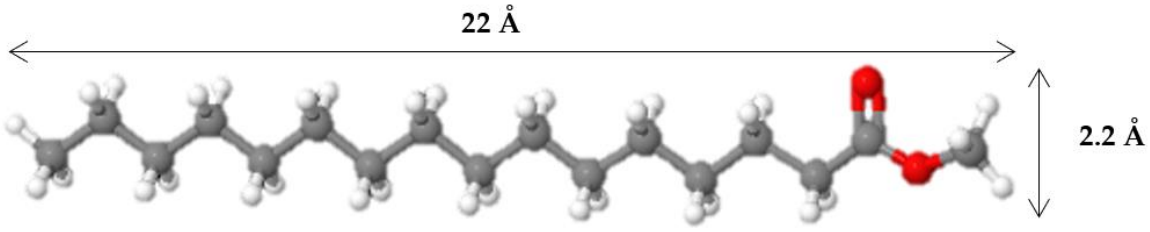

Figure 13. Dimensions of methyl palmitate. Gray, white, and red balls are carbon, hydrogen and oxygen atoms, respectively [54,55].

Preprints (www.preprints.org) | NOT PEER-REVIEWED | Posted: 19 September 2023 doi:10.20944/preprints202309.1239.v1

A temperature increase from 310 to 350 °C resulted in decrease of iso-alkanes yield over all MoS_2/Al_2O_3-zeolite catalysts: from 40% to 26% over MoS_2/Al_2O_3- ZSM-22; from 24% to 14% in the presence of MoS_2/Al_2O_3-SAPO-11 catalyst (Figure 12). Catalytic experiments showed that decrease of iso-alkanes yield with a temperature rise accompanied with increase of normal C_{16} and C_{15} alkanes while content of cracked products was changed slightly under the reaction conditions. Currently, we do not have a reasonable explanation for the observed dependence; a thorough study of the mechanism of ether and HDO intermediates transformation may help to elucidate this issue in future.

In addition, the effect of pressure (3.0 and 5.0 MPa) on the MP hydroisomerization over catalysts containing ZSM-22 zeolite and SAPO-11 was also investigated. The reaction was carried out at a temperature of 350°C, LHSV 36 h^{-1} and a H_2/feed ratio of 600 Nm^3/m^3. A pressure increase from 3.0 to 5.0 promoted MP conversion via 'direct' HDO route: HDO selectivity increased from 88.4 to 90.7% over MoS_2/Al_2O_3-SAPO-11 and from 85.4 to 88.9% over MoS_2/Al_2O_3-ZSM-22 catalyst, in consistence with previous results [15,24,46]. The yield of iso-alkanes decreases with pressure increase from 26% to 14.5% over MoS_2/ Al_2O_3-ZSM-22 catalyst and from 15% to 10% over MoS_2/Al_2O_3-SAPO-11 sample (Figure 14). The reason for this could be the acceleration of hydrogenation of olefins, which, according to the generally accepted mechanism, are intermediate products in hydroisomerization and hydrocracking reactions [13].

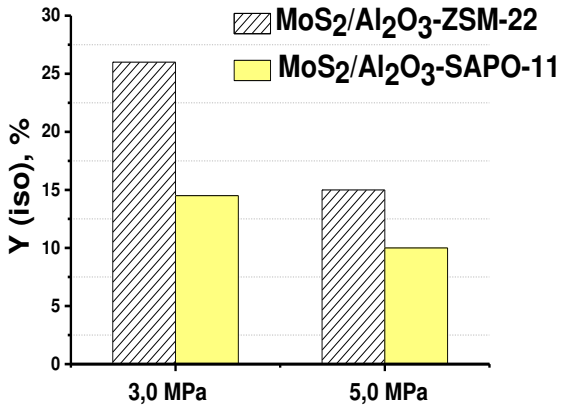

Figure 14. Pressure effect on yield of isomeric $C_{16}H_{34}$ and $C_{15}H_{32}$ alkanes over MoS_2/Al_2O_3-SAPO-11 and MoS_2/Al_2O_3-ZSM-22 catalysts (reaction conditions: 350°C, 3.0 and 5.0 MPa, 600 Nm^3/m^3, 36 h^{-1}).

In literature data pressure and temperature increase resulted in increase of the of iso-alkanes yield [56]. Authors performed MP hydrotreating at high temperature 350-410°C and pressure 6.0-12.0 MPa over sulfided $MoO_3/ZrPO_x$ in a batch reactor. So high temperatures activated the stable alkanes and yield of iso-alkanes increased. Our catalytic tests were performed at lower temperature and pressure range. A decrease in the activity of sulfide catalysts in the hydroisomerization of methyl palmitate was observed with increasing pressure and temperature, which is related to the reaction mechanism. The conversion of methyl palmitate over sulfide catalysts is quite complex, including hydrodeoxygenation and hydroisomerization reactions. Presumably, alkane isomers are formed not from the final product of hydrodeoxygenation (n-hexadecane), but from intermediate products of methyl palmitate conversion (alcohol and olefins).

4. Materials and Methods

4.1. Support preparation

Four high silica zeolite powders with different framework type were used to prepare catalysts (Table 4). All samples (except ZSM-12) were purchased from Zeolyst Corp.

The synthesis of zeolite ZSM-12 was carried out using the following reagents: a colloidal solution of silicon dioxide LUDOX HS-40 (40 wt. %, Sigma-Aldrich), aluminum sulfate octadecahydrate ($Al_2(SO_4)_3 \cdot 18H_2O$, Sigma-Aldrich, 99%), methyltriethylammonium chloride ($[CH_3N(C_2H_5)_3]Cl$, Sigma-Aldrich, 97 %, abbreviated [MTEA]Cl), sodium hydroxide (NaOH, Komponent-Reaktiv, 98%), and ammonium nitrate (NH_4NO_3, Khimmed, 98 %). Solution A, consisting of 12.6 g of distilled water,

Preprints (www.preprints.org) | NOT PEER-REVIEWED | Posted: 19 September 2023 doi:10.20944/preprints202309.1239.v1

0.4 g of $Al_2(SO_4)_3 \cdot 18H_2O$, 1 g of NaOH, and 3.3 g [MTEA]Cl used as a template, was stirred until all of the components became completely dissolved. Solution B, consisting of 25.2 g of a 40% (wt.) colloidal solution of silicon dioxide of the brand LUDOX HS-40 and 10.1 g of distilled water, was stirred until the reaction mixture was homogeneous. Solution A was dropped into solution B and stirred gently. The gel was poured into a Teflon liner and placed into the autoclave, which was heated at 155°C for 120 h. The product was filtered off, washed with distilled water, dried at 110°C for 12 h, and calcined at 550°C for 10 h (heating rate 1 deg·min^{-1}). To obtain the H-form of zeolite, the synthesized material was treated 3 time with a 1 M aqueous solution of NH_4NO_3 at 80°C for 17 h. The solid product was filtered off, washed with distilled water, dried at 110°C for 12 h, and calcined at 550°C for 8 h (heating rate 1 deg·min^{-1}).

Table 4. List of zeolites relevant to this work with details.

Material	SiO_2/Al_2O_3 Mole Ratio	Framework Type	Channels	Size of channels
ZSM-5	280	MFI	3D, 10 MR	5.3 x 5.6 Å [010] 5,1 x 5,5 Å [100] [57]
ZSM-12	280	MTW	1D, 12 MR	5.6 x 7.7 Å [010] [58]
ZSM-22	97	TON	1D, 10 MR	4.6 x 5.7 Å [001] [57]
SAPO-11	$SiO_2/Al_2O_3/P_2O_5$= 0.25/1.0/0.8	AEL	1D, 10 MR	3.9 x 6.3 Å [001] [59]

Alumina support was prepared by HNO_3 peptization of pseudoboehmite (Disperal 20, Sasol GmbH). Zeolite-containing granular supports were prepared by mixing of pseudoboehmite (Disperal 20, Sasol GmbH) and zeolite powders followed by peptization with nitric acid and then piston extrusion through a trefoil-shaped die. After extruding, support granules were dried at 110°C during 12 h and then were calcined at 550 °C in air flow during 6 h. Zeolite content was 30 wt.% in all calcined composite supports. Synthesized supports were denoted as Al_2O_3-ZSM-5, Al_2O_3-ZSM-12, Al_2O_3-ZSM-22 and Al_2O_3-SAPO-11.

4.2. Catalyst preparation

Mo catalysts were prepared by incipient wetness impregnation of synthesized alumina and zeolite-containing extrudates by aqua solution containing ammonium heptamolybdate ($(NH_4)_6Mo_7O_{24} \cdot 4H_2O$ from Vekton) and citric acid monohydrate ($C_6H_8O_7 \cdot H_2O$ from Vekton). Mo content was about 7.0 wt.% after calcination of the catalysts at 550°C for 4 hours.

4.3. Support and catalyst characterization

The textural properties of the synthesized supports were determined using nitrogen physisorption at 77K with an Autosorb-6B-Kr instrument ("Quantachrome Instruments", USA).

The elemental analysis was performed using inductively coupled plasma atomic emission spectroscopy (ICPAES) on Optima 4300 DV ("Perkin Elmer", France). The Mo content was determined after calcination of the catalysts at 550 °C for 4 h.

X-ray powder diffraction (XRD) patterns of supports and catalysts were obtained with an instrument STOE STADI MP ("STOE", Germany) with a detector MYTHEN2 1K using MoKα radiation (wave length λ = 0.7093Å). The measurements were carried out in a range of 2θ from 2 to 40° with scanning step of 0.015°.

Acidity of Al_2O_3-zeolite supports and pure Al_2O_3 were characterized by FTIR spectroscopy of adsorbed carbon monoxide. FTIR spectra were recorded on a Shimadzu FTIR-8300 spectrometer within the spectral range of 700–6000 cm^{-1}, resolution of 4 cm^{-1} and 300 scans for signal accumulation. The powder samples were pressed in thin self-supporting wafers of 0.010-0.012 g×cm^{-2} density and pretreated in the home made IR cell at 500°C for 2 h under dynamic vacuum of less than 10^{-3} Pa. In

Preprints (www.preprints.org) | NOT PEER-REVIEWED | Posted: 19 September 2023 doi:10.20944/preprints202309.1239.v1

the presented spectra, the absorbance was normalized to sample wafer density. CO was introduced at liquid nitrogen temperature by doses from low pressure of 0.1 mbar up to an equilibrium pressure of 10 mbar. The concentration of Brønsted acid sites (BAS) was determined from the integral intensity of the bands assigned to hydrogen bonded complexes of CO molecules with the OH–groups using the following molar integral absorption coefficients values: A_0=54 cm/μmol for the complexes with $\nu_{OH...CO}$ ~ 3280-3380 cm^{-1} and A_0=27 cm/μmol for the complexes with $\nu_{OH...CO}$ 3500 cm^{-1} [60].

Morphology of supports was studied using Hitachi Regulus SU8230 FESEM scanning electron microscope (Hitachi, Japan) with an accelerating voltage of 2 and 5 kV, in the modes of secondary (SE) and backscattered (BSE) electrons using an Upper (U) detector, which makes it possible to obtain microscopic images in phase and topographic contrasts. The study of the chemical composition was also carried out on a Hitachi Regulus SU8230 FESEM scanning electron microscope (Hitachi, Japan) with an accelerating voltage of 20 kV. The device is equipped with an AztecLive (Oxford Instruments, England) energy-dispersive X-ray characteristic spectrometer (EDX) with a semiconductor Si detector with an energy resolution of 128 eV.

The morphology of sulfide phase of the catalysts after hydroprocessing were studied by high-resolution transmission electron microscopy (HRTEM) using a ThemisZ electron microscope ("Thermo Fisher Scientific", USA) with an accelerating voltage of 200 kV and a limiting resolution of 0.07 nm. Images were recorded using a Ceta 16 CCD array ("Thermo Fisher Scientific", USA). The instrument is equipped with a SuperX ("Thermo Fisher Scientific", USA) energy-dispersive characteristic X-ray spectrometer (EDX) with a semiconductor Si detector with an energy resolution of 128 eV. To obtain statistical information, the structural parameters of ca. 500 particles were measured.

4.4. Catalytic experiments

The catalytic experiments were performed using an experimental setup with a trickle-bed reactor with an inner diameter 12 mm and length 370 mm. In each experiment 0.5 ml of catalyst (0.25–0.50 mm size fraction) was diluted with inert material, carborundum (0.1–0.25 mm size fraction) in a 1:8 volume ratio. Prior the catalytic experiments the catalysts were activated by in-situ sulfidation with dimethyl disulfide in dodecane (0.6 wt.% sulfur) at H_2 pressure – 3.5 MPa, H_2/feed ratio – 300 Nm^3/m^3 and LHSV – 20 h^{-1}. Sulfidation was performed at temperature 340°C during 4 h with a heating rate of 25°C/hour.

Hydroprocessing of methyl palmitate was carried out at temperature range 250-350°C, H_2 pressure 3.0 and 5.0 MPa, H_2/feed ratio – 600 Nm^3/m^3 and LHSV – 36 h^{-1}. The feed was 10 wt.% of methyl palmitate in dodecane (1.17 wt.% O). The duration of each step was 6 hours.

To check catalyst stability, oxygen conversion was compared in the first and the last stages carried out in the same conditions in each experiment (290°C, 3.0 MPa, H_2/feed ratio – 600 Nm^3/m^3 and LHSV – 36 h^{-1}.).

4.5. Product analysis

The products of methyl palmitate (MP) conversion were analyzed using an Agilent 6890N gas chromatograph ("Agilent Technologies", USA) equipped with a flame ionization detector and an HP-1MS quartz capillary column (30 m × 0.32 mm × 1 μm). Methyl palmitate conversion was calculated as (1):

$$X_{MP} = \frac{C^0_{MP} - C_{MP}}{C^0_{MP}} \times 100\%, \quad (1)$$

where C^0_{MP}– the chromatogram peak area of MP in the feed, C_O – the chromatogram peak area of MP in the final product.

The total oxygen content in liquid samples was determined using a Vario EL Cube elemental CHNSO analyzer ("Elementar Analysensysteme GmbH", Germany).

Oxygen conversion was calculated as (2):

$$X_O = \frac{C^0_O - C_O}{C^0_O} \times 100\%, \quad (2)$$

where C^0_O– total oxygen content in the feed, C_O – total oxygen content in the final product.

Gas phase during the MP hydroprocessing was analyzed online using a gas chromatograph Chromos 1000 ("Chromos", Russia) equipped with a methanator and a flame ionization detector.

Selectivity of 'direct' HDO route (HDO selectivity) was calculated as (3):

$$S = \frac{C_{16}}{C_{16}+C_{15}} \times 100\%, \quad (3)$$

where C_{16} – content of C_{16} alkanes (normal + iso) in final product; C_{15} – content of C_{15} alkanes (normal + iso) in final product.

Yield of iso-alkanes was calculated as (4):

$$Y(iso) = \frac{i-C_{16} + i-C_{15}}{\sum(C_{16} + C_{15})} * 100\%, \quad (4)$$

where *i*-C_{16} and *i*-C_{15} – content of *iso*-C_{16} and *iso*-C_{15} alkanes in final product at complete oxygen conversion; $\sum(C_{16} + C_{15})$- sum of normal and iso-alkanes at complete oxygen conversion.

5. Conclusions

Synthesized composite zeolite-containing supports (30 wt.% zeolite and 70% Al_2O_3) and corresponding sulfide Mo-containing catalysts were characterized by XRD, HRTEM and SEM. According to XRD data structure of zeolites was preserved in synthesized supports and catalysts. Uniform distribution of zeolite crystallites in composite materials (Al_2O_3-ZSM-5, Al_2O_3-ZSM-12, Al_2O_3-ZSM-22, Al_2O_3-SAPO-11) was confirmed by SEM-EDX. 100% conversion of oxygen was observed at temperature 310°C over sulfided Mo/Al_2O_3-zeolite catalysts in hydroprocessing of methyl palmitate. A temperature rise from 310 to 350°C resulted in decrease of HDO selectivity. It was found that the addition of zeolite to alumina has slight influence on MP conversion, but effect on conversion of oxygen-containing compounds is greater. Activity of MoS_2/Al_2O_3-zeolite catalysts in production of isomerized alkanes in MP hydroconversion is in good correlation with concentration of Brønsted acid sites. The yield of iso-alkanes in hydroisomerization of MP increased in the following order Al_2O_3<Al_2O_3-ZSM-12<Al_2O_3-ZSM-5<Al_2O_3-SAPO-11<Al_2O_3-ZSM-22. The yield of iso-alkanes was affected by temperature and hydrogen pressure. Increase of temperature and pressure resulted in decrease of iso-alkanes yield. This observation, probably, can be explained by reaction mechanism under the given reaction conditions: iso-alkanes are formed from intermediate products of methyl palmitate HDO, not from alkanes.

Supplementary Materials: The following supporting information can be downloaded at: www.mdpi.com/xxx/s1, Figure S1: FTIR spectra of CO adsorbed on pure Al_2O_3 and Al_2O_3-SAPO-11 supports. Equilibrium CO pressure is 5 mbar at liquid nitrogen temperature. Spectra normalized to the alumina content; Figure S2: FTIR difference spectra of the OH stretching region during adsorption of CO on Al_2O_3-ZSM-22 support. Equilibrium CO pressures used were from 0.3 (bottom curve) to 10 mbar (top curve).

Author Contributions: Data curation, writing—original draft preparation, E.V. and A.N.; investigation, Y.Z., I.S. and P.A., characterization by FTIR spectroscopy, I.D.; characterization by XRD, V.P.; characterization by SEM, E.S.; preparation of ZSM-12, D.T, supervision, A.M.; supervision, writing—review and editing, G.B. All authors have read and agreed to the published version of the manuscript.

Funding: This research was supported by the Russian Science Foundation, grant number 22-13-00371.

Institutional Review Board Statement: Not applicable.

Informed Consent Statement: Not applicable.

Data Availability Statement: Data is available upon request from the corresponding authors.

Acknowledgments: The authors are grateful to Dr. E.Yu. Gerasimov for HRTEM analysis.

Conflicts of Interest: The authors declare no conflict of interest

References

1. Panoutsou, C.; Germer, S.; Karka, P.; Papadokostantakis, S.; Kroyan, Y.; Wojcieszyk, M.; Maniatis, K.; Marchand, P.; Landalv, I., Advanced biofuels to decarbonise European transport by 2030: Markets, challenges, and policies that impact their successful market uptake. *Energy Strategy Reviews* **2021,** *34*.
2. Douvartzides, S. L.; Charisiou, N. D.; Papageridis, K. N.; Goula, M. A., Green Diesel: Biomass Feedstocks, Production Technologies, Catalytic Research, Fuel Properties and Performance in Compression Ignition Internal Combustion Engines. *Energies* **2019,** *12* (5).

3. Mittelbach, M., Fuels from oils and fats: Recent developments and perspectives. *European Journal of Lipid Science and Technology* **2015,** *117* (11), 1832-1846.
4. Vasquez, M. C.; Silva, E. E.; Castillo, E. F., Hydrotreatment of vegetable oils: A review of the technologies and its developments for jet biofuel production. *Biomass & Bioenergy* **2017,** *105*, 197-206.
5. Goh, B. H. H.; Chong, C. T.; Ge, Y.; Ong, H. C.; Ng, J.-H.; Tian, B.; Ashokkumar, V.; Lim, S.; Seljak, T.; Józsa, V., Progress in utilisation of waste cooking oil for sustainable biodiesel and biojet fuel production. *Energy Conversion and Management* **2020,** *223*, 113296.
6. Maki-Arvela, P.; Martinez-Klimov, M.; Murzin, D. Y., Hydroconversion of fatty acids and vegetable oils for production of jet fuels. *Fuel* **2021,** *306*.
7. Long, F.; Liu, W. G.; Jiang, X.; Zhai, Q. L.; Cao, X. C.; Jiang, J. C.; Xu, J. M., State-of-the-art technologies for biofuel production from triglycerides: A review. *Renewable & Sustainable Energy Reviews* **2021,** *148*.
8. Yeletsky, P. M.; Kukushkin, R. G.; Yakovlev, V. A.; Chen, B. H., Recent advances in one-stage conversion of lipid-based biomass-derived oils into fuel components - aromatics and isomerized alkanes. *Fuel* **2020,** *278*.
9. Hari, T. K.; Yaakob, Z., Production of diesel fuel by the hydrotreatment of jatropha oil derived fatty acid methyl esters over gamma-Al_2O_3 and SiO_2 supported NiCo bimetallic catalysts. *Reaction Kinetics Mechanisms and Catalysis* **2015,** *116* (1), 131-145.
10. Bezergianni, S.; Dimitriadis, A.; Chrysikou, L. P., Quality and sustainability comparison of one- vs. two-step catalytic hydroprocessing of waste cooking oil. *Fuel* **2014,** *118*, 300-307.
11. Hsu, H. W.; Chang, Y. H.; Wang, W. C., Techno-economic analysis of used cooking oil to jet fuel production under uncertainty through three-, two-, and one-step conversion processes. *Journal of Cleaner Production* **2021,** *289*.
12. Akhmedov, V. M.; Al-Khowaiter, S. H., Recent advances and future aspects in the selective isomerization of high n-alkanes. *Catalysis Reviews-Science and Engineering* **2007,** *49* (1), 33-139.
13. Qian, E. W.; Chen, N.; Gong, S., Role of support in deoxygenation and isomerization of methyl stearate over nickel-molybdenum catalysts. *Journal of Molecular Catalysis a-Chemical* **2014,** *387*, 76-85.
14. Li, X.; Fan, Q.; Wu, Y.; Lin, X.; Ma, S.; Li, S.; Ye, Y.; Wang, D.; Cheng, J.; Zheng, Z., Enhancing hydrodeoxygenation-isomerization of FAME over M-SAPO-11 in one-step process: Effect of in-situ isomorphic substitution of transition metals and synergy of PtxSny alloy. *Chemical Engineering Journal* **2023,** *452*, 139528.
15. Chen, L. G.; Li, H. W.; Fu, J. Y.; Miao, C. L.; Lv, P. M.; Yuan, Z. H., Catalytic hydroprocessing of fatty acid methyl esters to renewable alkane fuels over Ni/HZSM-5 catalyst. *Catalysis Today* **2016,** *259*, 266-276.
16. Cheng, J.; Zhang, Z.; Zhang, X.; Fan, Z. T.; Liu, J. F.; Zhou, J. H., Continuous hydroprocessing of microalgae biodiesel to jet fuel range hydrocarbons promoted by Ni/hierarchical mesoporous Y zeolite catalyst. *INTERNATIONAL JOURNAL OF HYDROGEN ENERGY* **2019,** *44* (23), 11765-11773.
17. Cheng, J.; Zhang, Z.; Zhang, X.; Liu, J. F.; Zhou, J. H.; Cen, K. F., Hydrodeoxygenation and hydrocracking of microalgae biodiesel to produce jet biofuel over H3PW12O40-Ni/hierarchical mesoporous zeolite Y catalyst. *Fuel* **2019,** *245*, 384-391.
18. Zhang, Z.; Cheng, J.; Zhu, Y. X.; Guo, H.; Yang, W. J., Jet fuel range hydrocarbons production through competitive pathways of hydrocracking and isomerization over HPW-Ni/MCM-41 catalyst. *Fuel* **2020,** *269*.
19. Li, T.; Cheng, J.; Zhang, X.; Liu, J. F.; Huang, R.; Zhou, J. H., Jet range hydrocarbons converted from microalgal biodiesel over mesoporous zeolite-based catalysts. *INTERNATIONAL JOURNAL OF HYDROGEN ENERGY* **2018,** *43* (21), 9988-9993.
20. Xiao, Y.; Shang, J.; Zhai, M.; Qiao, C., Hydrodeoxygenation of fatty acid methyl esters and simultaneous products isomerization over bimetallic Ni-Co/SAPO-11 catalysts. *International Journal of Energy Research* **2021,** *45* (6), 9648-9656.
21. Zhao, S.; Li, M.; Chu, Y.; Chen, J., Hydroconversion of Methyl Laurate as a Model Compound to Hydrocarbons on Bifunctional Ni2P/SAPO-11: Simultaneous Comparison with the Performance of NUSAPO-11. *Energy & Fuels* **2014,** *28* (11), 7122-7132.
22. Cai, Z.; Ding, Y.; Zhang, J.; Yu, P.; Ma, Y.; Cao, Y.; Zheng, Y.; Huang, K.; Jiang, L., In situ generation of dispersed MoS2 catalysts from oil-soluble Mo-based ionic liquids for highly effective biolipids hydrodeoxygenation. *Journal of Catalysis* **2023,** *423*, 50-61.
23. Deliy, I. V.; Vlasova, E. N.; Nuzhdin, A. L.; Gerasimov, E. Y.; Bukhtiyarova, G. A., Hydrodeoxygenation of methyl palmitate over sulfided Mo/Al2O3, CoMo/Al2O3 and NiMo/Al2O3 catalysts. *Rsc Advances* **2014,** *4* (5), 2242-2250.
24. Kaluza, L.; Kubicka, D., The comparison of Co, Ni, Mo, CoMo and NiMo sulfided catalysts in rapeseed oil hydrodeoxygenation. *Reaction Kinetics Mechanisms and Catalysis* **2017,** *122* (1), 333-341.
25. Dupont, C.; Lemeur, R.; Daudin, A.; Raybaud, P., Hydrodeoxygenation pathways catalyzed by MoS2 and NiMoS active phases: A DFT study. *Journal of Catalysis* **2011,** *279* (2), 276-286.
26. Kubickova, I.; Kubicka, D., Utilization of Triglycerides and Related Feedstocks for Production of Clean Hydrocarbon Fuels and Petrochemicals: A Review. *Waste and Biomass Valorization* **2010,** *1* (3), 293-308.

27. Bergwerff, J. A.; Jansen, M.; Visser, T.; de Jong, K. P.; Weckhuysen, B. M., Influence of the preparation method on the hydrotreating activity of MoS2/Al2O3 extrudates: A Raman microspectroscopy study on the genesis of the active phase. *Journal of Catalysis* **2006,** *243* (2), 292-302.
28. Busca, G., Structural, surface, and catalytic properties of aluminas. In *Advances in catalysis*, Elsevier: 2014; Vol. 57, pp 319-404.
29. Meriaudeau, P.; Tuan, V.; Nghiem, V. T.; Lai, S.; Hung, L.; Naccache, C., SAPO-11, SAPO-31, and SAPO-41 molecular sieves: synthesis, characterization, and catalytic properties inn-octane hydroisomerization. *Journal of Catalysis* **1997,** *169* (1), 55-66.
30. Morterra, C.; Magnacca, G.; Demaestri, P., Surface characterization of modified aluminas: III. Surface-features of PO4-doped Al2O3. *Journal of Catalysis* **1995,** *152* (2), 384-395.
31. Verboekend, D.; Chabaneix, A. M.; Thomas, K.; Gilson, J.-P.; Pérez-Ramírez, J., Mesoporous ZSM-22 zeolite obtained by desilication: peculiarities associated with crystal morphology and aluminium distribution. *CrystEngComm* **2011,** *13* (10), 3408-3416.
32. Kustov, L.; Kazanskii, V.; Beran, S.; Kubelkova, L.; Jiru, P., Adsorption of carbon monoxide on ZSM-5 zeolites: infrared spectroscopic study and quantum-chemical calculations. *Journal of Physical Chemistry* **1987,** *91* (20), 5247-5251.
33. Dimitrov, L.; Mihaylov, M.; Hadjiivanov, K.; Mavrodinova, V., Catalytic properties and acidity of ZSM-12 zeolite with different textures. *Microporous and Mesoporous Materials* **2011,** *143* (2-3), 291-301.
34. Gabrienko, A. A.; Danilova, I. G.; Arzumanov, S. S.; Toktarev, A. V.; Freude, D.; Stepanov, A. G., Strong acidity of silanol groups of zeolite beta: Evidence from the studies by IR spectroscopy of adsorbed CO and 1H MAS NMR. *Microporous and Mesoporous Materials* **2010,** *131* (1-3), 210-216.
35. Morterra, C.; Bolis, V.; Magnacca, G., IR spectroscopic and microcalorimetric characterization of Lewis acid sites on (transition phase) Al2O3 using adsorbed CO. *Langmuir* **1994,** *10* (6), 1812-1824.
36. Zecchina, A.; Bordiga, S.; Spoto, G.; Scarano, D., Petrini, G., Leofanti, G., Padovan, M., Otero Areàn, C., Low-temperature Fourier-transform Infrared Investigation of the Interaction of CO with Nanosized ZSM5 and Silicalite . *J. CHEM. SOC. FARADAY TRANS*. **1992**, *88* (19), 2959-2969
37. Gabrienko, A. A.; Danilova, I. G.; Arzumanov, S. S.; Freude, D.; Stepanov, A. G., Does the Zn2+ Species Introduced into H-ZSM-5 Zeolite Affect the Strength of Brønsted Acid Sites? *Chemcatchem* **2020,** *12* (2), 478-487.
38. Kwak, S. H. Spectroscopic characterization of the surface hydroxyls of zeolitic catalysts. 2014.
39. Hadjiivanov, K., Identification and characterization of surface hydroxyl groups by infrared spectroscopy. In *Advances in Catalysis*, Elsevier: 2014; Vol. 57, pp 99-318.
40. Chakarova, K.; Hadjiivanov, K., Problems in the IR measuring the acidity of zeolite bridging hydroxyls by low-temperature CO adsorption. *Chemical Communications* **2011,** *47* (6), 1878-1880.
41. Höchtl, M.; Jentys, A.; Vinek, H., Acidity of SAPO and CoAPO molecular sieves and their activity in the hydroisomerization of n-heptane. *Microporous and Mesoporous Materials* **1999,** *31* (3), 271-285.
42. Nazimov, D.; Klimov, O.; Danilova, I.; Trukhan, S.; Saiko, A.; Cherepanova, S.; Chesalov, Y. A.; Martyanov, O.; Noskov, A., Effect of alumina polymorph on the dehydrogenation activity of supported chromia/alumina catalysts. *Journal of Catalysis* **2020,** *391*, 35-47.
43. de Brimont, M. R.; Dupont, C.; Daudin, A.; Geantet, C.; Raybaud, P., Deoxygenation mechanisms on Ni-promoted MoS2 bulk catalysts: A combined experimental and theoretical study. *Journal of Catalysis* **2012,** *286*, 153-164.
44. Vlasova, E. N.; Bukhtiyarova, G. A.; Deliy, I. V.; Aleksandrov, P. V.; Porsin, A. A.; Panafidin, M. A.; Gerasimov, E. Y.; Bukhtiyarov, V. I., The effect of rapeseed oil and carbon monoxide on SRGO hydrotreating over sulfide CoMo/Al2O3 and NiMo/Al2O3 catalysts. *Catalysis Today* **2020,** *357*, 526-533.
45. Coumans, A. E.; Hensen, E. J. M., A model compound (methyl oleate, oleic acid, triolein) study of triglycerides hydrodeoxygenation over alumina-supported NiMo sulfide. *Applied Catalysis B-Environmental* **2017,** *201*, 290-301.
46. Yoosuk, B.; Sanggam, P.; Wiengket, S.; Prasassarakich, P., Hydrodeoxygenation of oleic acid and palmitic acid to hydrocarbon-like biofuel over unsupported Ni-Mo and Co-Mo sulfide catalysts. *Renewable Energy* **2019,** *139*, 1391-1399.
47. Zhang, M.; Chen, Y. J.; Wang, L.; Zhang, Q. M.; Tsang, C. W.; Liang, C. H., Shape Selectivity in Hydroisomerization of Hexadecane over Pt Supported on 10-Ring Zeolites: ZSM-22, ZSM-23, ZSM-35, and ZSM-48. *Industrial & Engineering Chemistry Research* **2016,** *55* (21), 6069-6078.
48. Lanzafame, P.; Perathoner, S.; Centi, G.; Heracleous, E.; Iliopoulou, E. F.; Triantafyllidis, K. S.; Lappas, A. A., Effect of the Structure and Mesoporosity in Ni/Zeolite Catalysts for n-Hexadecane Hydroisomerisation and Hydrocracking. *Chemcatchem* **2017,** *9* (9), 1632-1640.
49. Valtchev, V.; Majano, G.; Mintova, S.; Pérez-Ramírez, J., Tailored crystalline microporous materials by post-synthesis modification. *Chemical Society Reviews* **2013,** *42* (1), 263-290.

50. Pérez-Ramírez, J.; Christensen, C. H.; Egeblad, K.; Christensen, C. H.; Groen, J. C., Hierarchical zeolites: enhanced utilisation of microporous crystals in catalysis by advances in materials design. *Chemical Society Reviews* **2008,** *37* (11), 2530-2542.
51. Schwieger, W.; Machoke, A. G.; Weissenberger, T.; Inayat, A.; Selvam, T.; Klumpp, M.; Inayat, A., Hierarchy concepts: classification and preparation strategies for zeolite containing materials with hierarchical porosity. *Chemical Society Reviews* **2016,** *45* (12), 3353-3376.
52. Roth, W. J.; Nachtigall, P.; Morris, R. E.; Cejka, J., Two-dimensional zeolites: current status and perspectives. *Chemical Reviews* **2014,** *114* (9), 4807-4837.
53. Jang, H.-G.; Min, H.-K.; Lee, J. K.; Hong, S. B.; Seo, G., SAPO-34 and ZSM-5 nanocrystals' size effects on their catalysis of methanol-to-olefin reactions. *Applied Catalysis A: General* **2012,** *437*, 120-130.
54. http://www.chemspider.com/Chemical-Structure.7889. Available online: URL (accessed on 4 September 2023).
55. https://avogadro.cc/. Available online: URL (accessed on 4 September 2023).
56. Cai, Z.; Wang, Y.; Cao, Y.; Yu, P.; Ding, Y.; Ma, Y.; Zheng, Y.; Huang, K.; Jiang, L., Direct production of isomerized biodiesel over MoS2/ZrPOx under solvent-free conditions. *Fuel* **2023,** *337*, 127175.
57. https://asia.iza-structure.org. Available online: URL (accessed on 4 September 2023).
58. Fyfe, C.; Gies, H.; Kokotailo, G.; Marler, B.; Cox, D., Crystal structure of silica-ZSM-12 by the combined use of hgh-resolution solid-state MAS NMR spectroscopy and synchrotron x-ray powder diffraction. *Journal of Physical Chemistry* **1990,** *94* (9), 3718-3721.
59. Borade, R. B.; Clearfield, A., A comparative study of acidic properties of SAPO-5,− 11,− 34 and− 37 molecular sieves. *Journal of molecular catalysis* **1994,** *88* (2), 249-265.
60. Dik, P.; Klimov, O.; Danilova, I.; Leonova, K.; Pereyma, V. Y.; Budukva, S.; Uvarkina, D.; Kazakov, M.; Noskov, A., Hydroprocessing of hydrocracker bottom on Pd containing bifunctional catalysts. *Catalysis Today* **2016,** *271*, 154-162